Bridging properties of the debonded interface with frictional sliding*

LIU Pengfei[1], TAO Weiming[1]**, YU Xuezhong[2] and GUO Yimu[1]

(1. Department of Engineering Mechanics, Zhejiang University, Hangzhou 310027, China; 2. Second Affiliated Hospital, Zhejiang University, Hangzhou 310009, China)

Received April 25, 2005; revised July 19, 2005

Abstract A theoretical model simulating the properties of frictional bridging is presented and relatively perfect stress solutions for the fiber and matrix are obtained. Based on the energy equilibrium in the process of interfacial debonding, an expression for the energy release rate G is derived to explore the interfacial fracture properties. By introducing an interfacial debonding criterion $G \geqslant \Gamma_i$, a method for determining the critical debond length is proposed and the bridging constitutive relationship is also obtained. Numerical calculations are conducted for the fiber-reinforced composite SCS-6/T_i-6Al-4V and the results are also compared with those obtained by using other existing models.

Keywords: interfacial stress transfer, frictional sliding, energy release rate, bridging constitutive relationship, fiber-reinforced composites.

An important toughening mechanism is bridging of matrix cracks by fibers in fiber-reinforced composites, where complicated friction and sliding occur at the debonded interface. The mechanical performances of composites depend mainly on the interfacial properties, which are relevant to the development of different types of failure[1,2].

Because the bridging loads exerted by fibers on matrix cracks are pull-out loads for fibers, micromechanical test on fiber pull-out has become a widely used method for exploring the properties of interfacial fracture and failure. For the study of fiber pull-out, the interfacial-shear- strength-based criterion is questionable, which arises mainly from two reasons: (1) The criterion depends on practical models and may be used only for qualitative comparisons of various interfaces; (2) Hampe[3] and Piggott[4] pointed out from experimental studies that a debonded interface may appear before the interfacial shear stress reaches the interfacial shear strength. By contrast, according to the energy-based interfacial debonding criterion, the interface crack is assumed to propagate when the energy release rate G exceeds the interfacial debonding toughness Γ_i, where G is interpreted as the energy changes when the interface crack with the length of L_d advances a length dL_d. The energy-based debonding criterion has been verified to be more superior than the shear-strength-based criterion[5,6].

Because the energy-based interfacial debonding criterion depends on the stress and strain fields at the debonded and bonded regions, accurate predictions of the stress distributions in the fiber and matrix are very important. Jiang[7] and Hsueh[8] applied the shear-lag models, and Liu[9] applied the Lamé method to derive expressions for the energy release rate G. However, they neglected some terms such as the shear stress and strain energy in the fiber, the interfacial radial stress, the variations of axial stress in the matrix with the radial positions, the axial displacements in the fiber and matrix at the bonded regions, and the Poisson's effect, etc. By averaging the axial stress in the matrix only as a function of the axial positions, Chiang[10] derived an expression for the energy release rate G, including the axial strain energies in the fiber, and the axial and shear strain energies in the matrix. Rauchs et al.[11,12] obtained numerical solutions of the energy release rate G by using the finite element method. However, their oversimplifications resulted in severe errors. Quek[13] obtained numerical solutions of the release rate of the strain energy by employing stress functions. However, some terms were neglected, such as the work done by the friction stress, the axial and radial displacement continuity conditions in the fiber and ma-

* Supported by Natural Science Foundation of Zhejiang Province (Grant No. M503095)

** To whom correspondence should be addressed. E-mail: taowm@zju.edu.cn

trix at the bonded interface, the Poisson's effect, and the shear strain energy in the fiber, etc.

In this paper, we give all the stress solutions in the fiber and matrix with friction at the debonded interface obtained by introducing stress equilibrium equations, the boundary- and continuity- conditions. Based on the energy equilibrium between the work U_w done by the pull-out stress σ_b, the work U_f done by the friction stress τ_s, the strain energy U_e in the fiber and matrix, and the interfacial debonding energy U_s, expressions for the energy release rate G and bridging constitutive relationship are derived. The established model includes the axial, shear and radial stresses in the fiber and matrix, the axial displacements in the bonded and debonded regions, the thermal residual stresses due to the fiber/matrix thermal mismatch, and the Poisson's effect, which ensures its high accuracy.

1 Interfacial stress analysis

Fig. 1 shows a composite specimen loaded by bidirectional symmetric stresses, wherein an I-type matrix crack is bridged by parallel fibers. Frictional sliding occurs at position x at the debonded interface, a distance from the matrix crack tip. The axial displacement mismatch between the fiber and the matrix leads to the formation of matrix crack opening displacement (COD) profile $2u(x)$.

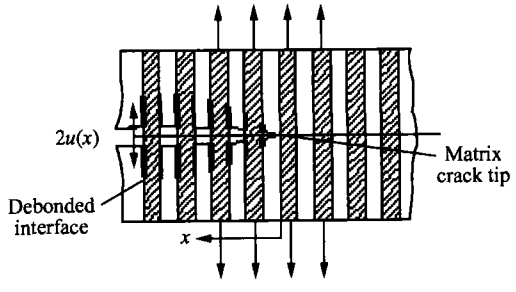

Fig. 1. Schematic diagram of an I-type matrix crack bridged by parallel fibers.

A single fiber embedded in a concentric cylindrical matrix is extracted from Fig.1, as shown in Fig.2. The fiber volume fraction is $V_f = r_1^2/r_2^2$ and the matrix volume fraction is $V_m = 1 - V_f$. L is the embedded fiber length and L_d is the interface debond length. Both the fiber and matrix are considered to be linear-elastic and transversely isotropic. A cylindrical coordinate (r, θ, z) is defined and the z axis represents the fiber axial direction. The loaded and embedded ends are $z = 0$ and $z = L$, respectively. The pull-out stress σ_b is parallel to the z axis.

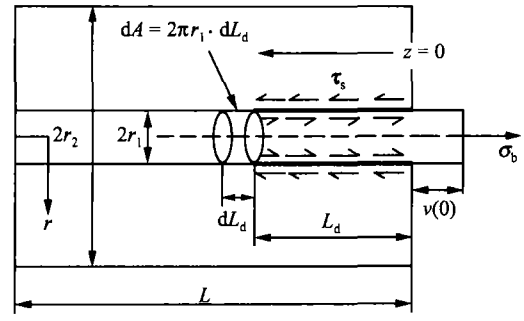

Fig. 2. Frictional sliding at the debonded interface under the pull-out stress.

The equilibrium between the fiber axial stress $\sigma_f^z(z)$ and the interfacial shear stress $\tau_i(z)$ requires

$$\frac{d\sigma_f^z(z)}{dz} = -\frac{2}{r_1}\tau_i(z), \tag{1}$$

where $\sigma_f^z(z)$ is considered to be an average axial stress on the fiber cross section.

The equilibrium between the axial stresses in the fiber and matrix requires

$$V_f\sigma_b = V_m\sigma_m^z(z) + V_f\sigma_f^z(z). \tag{2}$$

According to Hsueh[8] and Chiang[14], if an average constant friction stress τ_s along the debonded interface is determined by the interfacial roughness effect, combining Eqs. (1) and (2), we can obtain

$$\sigma_f^z(z) = \sigma_b - \frac{2\tau_s}{r_1}z, \tag{3}$$

$$\sigma_m^z(z) = \frac{V_f}{V_m}\frac{2\tau_s}{r_1}z = \frac{2\lambda\tau_s}{r_1}z. \tag{4}$$

For 3D axisymmetric problems in the cylindrical coordinate, four non-zero stress components are unknown: σ^r, σ^θ, σ^z, $\sigma^{rz} = \sigma^{zr}$ except $\sigma^{r\theta} = \sigma^{\theta r} = 0$, $\sigma^{\theta z} = \sigma^{z\theta} = 0$. The equilibrium equations governing the axisymmetric stress solutions are expressed as

$$\frac{\partial\sigma_i^r}{\partial r} + \frac{\partial\tau_i^{rz}}{\partial z} + \frac{\sigma_i^r - \sigma_i^\theta}{r} = 0, \tag{5a}$$

$$\frac{\partial\sigma_i^z}{\partial z} + \frac{\partial\tau_i^{rz}}{\partial r} + \frac{\tau_i^{rz}}{r} = 0. \tag{5b}$$

The stress-strain relationships including the thermal effect are written as

$$\varepsilon_i^r = \frac{\partial u_i^r}{\partial r} = \frac{1}{E_i}[\sigma_i^r - \nu_i(\sigma_i^z + \sigma_i^\theta)] + \alpha_i^T\Delta T_p, \tag{6a}$$

$$\varepsilon_i^{\theta} = \frac{u_i^r}{r} = \frac{1}{E_i}[\sigma_i^{\theta} - \nu_i(\sigma_i^z + \sigma_i^r)] + \alpha_i^{T}\Delta T_p, \tag{6b}$$

$$\varepsilon_i^z = \frac{\partial u_i^z}{\partial z} = \frac{1}{E_i}[\sigma_i^z - \nu_i(\sigma_i^r + \sigma_i^{\theta})] + \alpha_i^{L}\Delta T_p, \tag{6c}$$

$$\gamma_i^{rz} \approx \frac{\partial u_i^z}{\partial r} = \frac{2(1+\nu_i)}{E_i}\tau_i^{rz}, \tag{6d}$$

where i = f, m represent the fiber and matrix, respectively; u and σ are the displacement and stress, respectively; E and ν stand for the elastic modulus and Poisson's ratio, respectively; α is the thermal expansion coefficient; the superscripts T and L denote the transverse and longitudinal directions, respectively; ΔT_p is the temperature change from the room temperature due to thermal processing and $\Delta T_p < 0$; the superscripts r, θ, rz and zr represent the radial, circumferential and tangential directions, respectively.

2 Boundary conditions of stresses and displacements

$$\sigma_f^z(z = L_d) = \sigma_b - \frac{2\tau_s L_d}{r_1} = \sigma_d, \tag{7a}$$

$$\sigma_m^z(z = L_d) = \frac{2\lambda\tau_s L_d}{r_1}, \tag{7b}$$

$$\sigma_f^r(r = r_1, z) = \sigma_m^r(r = r_1, z), \tag{7c}$$

$$\tau_f^{rz}(r = r_1, z) = \tau_m^{rz}(r = r_1, z) = \tau_i(z), \tag{7d}$$

$$\sigma_m^r(r = r_2, z) = 0, \tag{7e}$$

$$\tau_m^{rz}(r = r_2, z) = 0, \tag{7f}$$

$$u_f^r(r = r_1, z) = u_m^r(r = r_1, z), \tag{7g}$$

$$u_f^z(r = r_1, z) = u_m^z(r = r_1, z), \tag{7h}$$

where Eqs. (7a) and (7b) represent the continuity conditions of axial stresses in the fiber and matrix at the crack tip $z = L_d$, respectively; Eqs. (7c) and (7d) stand for the continuity conditions of radial and shear stresses in the fiber and matrix at the bonded interface, respectively; Eqs. (7e) and (7f) denote the boundary conditions of radial and shear stresses in the matrix at $r = r_2$, respectively; Eqs. (7g) and (7h) are the continuity conditions of radial and axial displacements in the fiber and matrix at the bonded interface, respectively; σ_d is the axial stress in the fiber at $z = L_d$.

In comparison, Quek[13] neglected Eqs. (7g) and (7h), and directly adopted Eqs. (7a)—(7f) and the fiber-field axial stresses in the fiber and matrix as boundary conditions for stress solutions.

3 Stress solutions

When $\sigma_f^r(z) = \sigma_f^{\theta}(z)$ is assumed for the fiber, Eqs. (6b) and (6c) can be further expressed as

$$\frac{u_f^r}{r} = \frac{1}{E_f}[(1-\nu_f)\sigma_f^r(z) - \nu_f\sigma_f^z(z)] + \alpha_f^{T}\Delta T_p, \tag{8}$$

$$\frac{\partial u_f^z}{\partial z} = \frac{1}{E_f}[\sigma_f^z(z) - 2\nu_f\sigma_f^r(z)] + \alpha_f^{L}\Delta T_p. \tag{9}$$

From Eqs. (1), (2), (5a), (7d) and (7f), the matrix shear stress $\tau_m^{rz}(r, z)$ can be solved

$$\tau_m^{rz}(r, z) = \frac{\lambda(r_2^2 - r^2)}{r_1 r}\tau_i(z). \tag{10}$$

By combining Eqs. (6c), (6d) and (10), and integrating the variable r, we can obtain

$$\sigma_m^r(r, z) + \sigma_m^{\theta}(r, z) = -\frac{\lambda}{r_1}\frac{2(1+\nu_m)}{\nu_m}\left(r_2^2\ln r - \frac{r^2}{2}\right)\frac{d\tau_i(z)}{dz} + 2f_1(z) + \alpha_m^{L}E_m\Delta T_p/\nu_m. \tag{11}$$

By combining Eqs. (5a), (7c), (7e), (8), (9) (10) and (11), and integrating the variable r, the matrix radial stress $\sigma_m^r(r, z)$ is solved

$$\sigma_m^r(r, z) = -\frac{\lambda r_2^2}{r_1}\left[-\frac{1}{2\nu_m} + \frac{1+\nu_m}{\nu_m}\ln r - \frac{1+2\nu_m}{4\nu_m}(r/r_2)^2\right]\frac{d\tau_i(z)}{dz} + f_2(z)/r^2 + f_1(z) + \alpha_m^{L}E_m\Delta T_p/2\nu_m, \tag{12}$$

where the functions $f_1(z)$ and $f_2(z)$ are expressed respectively as

$$f_1(z) = -\lambda\sigma_f^r(z) + \frac{r_2^2}{r_1}\frac{d\tau_i(z)}{dz}\left\{\lambda^2\left[\frac{1+\nu_m}{\nu_m}\ln(r_2/r_1) + \frac{(1+2\nu_m)}{4\nu_m}(r_1^2/r_2^2 - 1)\right] + \lambda\left[-\frac{3+2\nu_m}{4\nu_m} + \frac{1+\nu_m}{\nu_m}\ln r_2\right]\right\} - \alpha_m^{L}E_m\Delta T_p/2\nu_m, \tag{13}$$

$$f_2(z) = \lambda r_2^2\left\{\sigma_f^r(z) - \frac{\lambda r_2^2}{r_1}\frac{d\tau_i(z)}{dz}\left[\frac{1+\nu_m}{\nu_m}\ln(r_2/r_1)\right.\right.$$

$$+\frac{(1+2\nu_m)}{4\nu_m}(r_1^2/r_2^2-1)\Big]\Big\}. \quad (14)$$

From Eqs. (11)—(14), the matrix radial and circumferential stresses can be obtained

$$\sigma_m^r(r,z)=\frac{\lambda r_2^2}{r_1}\frac{d\tau_i(z)}{dz}\Big\{\frac{1+\nu_m}{\nu_m}[\ln(r_2/r)-\lambda(r_2^2/r^2-1)\ln(r_2/r_1)]-\frac{1+2\nu_m}{4\nu_m}(1-r^2/r_2^2)(1-r_1^2/r^2)\Big\}+\lambda(r_2^2/r^2-1)\sigma_f^r(z), \quad (15)$$

$$\sigma_m^\theta(r,z)=\frac{\lambda r_2^2}{r_1}\frac{d\tau_i(z)}{dz}\Big\{\frac{1+\nu_m}{\nu_m}[\ln(r_2/r)+\lambda(1+r_2^2/r^2)\ln(r_2/r_1)]-\frac{1+2\nu_m}{4\nu_m}(1+r^2/r_2^2)(1+r_1^2/r^2)-\frac{1+\nu_m}{\nu_m}(1-r^2/r_2^2)+1\Big\}-\lambda(1+r_2^2/r^2)\sigma_f^r(z)+\alpha_m^L E_m\Delta T_p/\nu_m. \quad (16)$$

By combining Eqs. (6a), (6b), (7g), (7h), (9), (15) and (16), a differential equation of the fiber axial stress $\sigma_f^z(z)$ is obtained

$$\frac{d^2\sigma_f^z(z)}{dz^2}-M\sigma_f^z(z)=-N, \quad (17)$$

where the coefficients M and N are expressed respectively as

$$M=[E_m(1-2\lambda_1\nu_f)/E_f+\lambda(1-2\lambda_1\nu_m)]/(\lambda_2-\lambda_1\lambda_3), \quad (18a)$$

$$N=\{\lambda(1-2\lambda_1\nu_m)\sigma_b+[2\lambda_1(\alpha_m^T+\alpha_m^L/\nu_m-\alpha_f^T)-\alpha_f^L]E_m\Delta T_p\}/(\lambda_2-\lambda_1\lambda_3), \quad (18b)$$

$$\lambda_1=(E_m\nu_f/E_f+\lambda\nu_m)/[E_m(1-\nu_f)/E_f+2\lambda+\nu_m+1], \quad (18c)$$

$$\lambda_2=\nu_m\lambda r_2^2\Big\{\frac{1+\nu_m}{\nu_m}\ln(r_2/r_1)(1+\lambda)-\frac{1+2\nu_m}{4\nu_m}(1+r_1^2/r_2^2)-\frac{1+\nu_m}{2\nu_m}(1-r_1^2/r_2^2)+1/2\Big\}, \quad (18d)$$

$$\lambda_3=\lambda r_2^2\Big\{\frac{1+\nu_m}{\nu_m}\ln(r_2/r_1)[1+\lambda(1+r_2^2/r_1^2)]-\frac{1+2\nu_m}{2\nu_m}(1+r_1^2/r_2^2)-\frac{1+\nu_m}{\nu_m}(1-r_1^2/r_2^2)+1\Big\}. \quad (18e)$$

By applying the stress continuity conditions in Eqs. (7a) and (7b), the fiber axial stress $\sigma_f^z(z)$ in the bonded regions is obtained

$$\sigma_f^z(z)=C\exp[-\beta(z-L_d)]+\sigma_f^\infty,\quad \sigma_f^\infty=N/M, \quad (19)$$

where the coefficients C and β are expressed respectively as

$$C=\sigma_d-\sigma_f^\infty=\sigma_b-\sigma_f^\infty-2\tau_s L_d/r_1,\quad \beta^2=M. \quad (20)$$

It should be pointed out that the far-field fiber axial stress $\sigma_f^\infty=E_fV_f\sigma_b/E_c$ obtained by Chiang[14] and Budiansky[15] is a special case of neglecting Poisson's effect or thermal effect in Eq. (19). The thermal effect including the Poisson's effect is determined by the transverse and longitudinal thermal expansions in the fiber and matrix. However, the thermal effect neglecting the Poisson's effect is determined only by the longitudinal thermal expansion in the fiber.

Substituting Eqs. (1) into (19), the shear stress $\tau_i(z)$ at the bonded interface is

$$\tau_i(z)=\frac{r_1}{2}C\beta\exp[-\beta(z-L_d)]. \quad (21)$$

From Eqs. (5) and (19), the fiber shear stress $\tau_f^{rz}(r,z)$ in the bonded regions is

$$\tau_f^{rz}(r,z)=\frac{r}{r_1}\tau_i(z)=\frac{C\beta r}{2}\exp[-\beta(z-L_d)]. \quad (22)$$

Combining Eqs. (7d) and (19), the matrix axial stress $\sigma_m^z(r,z)$ in the bonded regions can be obtained:

$$\sigma_m^z(r,z)=\sigma_m^\infty-\lambda C\exp[-\beta(z-L_d)],\quad \sigma_m^\infty=\lambda(\sigma_b-\sigma_f^\infty). \quad (23)$$

Combining Eqs. (21) and (10), the matrix shear stress $\tau_m^{rz}(r,z)$ in the bonded regions is

$$\tau_m^{rz}(r,z)=\frac{\lambda C\beta(r_2^2-r^2)}{2r}\exp[-\beta(z-L_d)]. \quad (24)$$

4 Interfacial debonding criteria

Four energy terms satisfy the following equilibrium relationship in the process of interfacial debonding:

$$U_w=U_e+U_f+U_s, \quad (25)$$

where $U_e=U_{ed}+U_{eb}$ is the sum of strain energies in

the debonded and bonded regions, U_f is the work done by the friction stress τ_s, U_w is the work done by the pull-out stress σ_b, and U_s is the interfacial debonding energy.

From Eqs. (3), (4), (19) and (22)—(24), U_{ed} and U_{eb} are calculated respectively by

$$\begin{aligned}U_{ed}=&\int_0^{L_d}\int_0^{r_1}\left[\frac{(\sigma_f^z(z))^2}{2E_f}+\frac{(\tau_f^z(r,z))^2}{2G_f}\right]2\pi r\mathrm{d}r\mathrm{d}z\\&+\int_0^{L_d}\int_{r_1}^{r_2}\left[\frac{(\sigma_m^z(r,z))^2}{2E_m}+\frac{(\tau_m^z(r,z))^2}{2G_m}\right]2\pi r\mathrm{d}r\mathrm{d}z\\=&\frac{\pi r_1^2}{2E_f}\left(\sigma_b^2L_d-\frac{2\tau_s\sigma_bL_d^2}{r_1}+\frac{4\tau_s^2L_d^3}{3r_1^2}\right)\\&+\frac{\pi r_1^2\tau_s^2L_d}{4G_f}+\frac{2\pi\lambda\tau_s^2L_d^3}{3E_m}+\frac{\pi\lambda^2\tau_s^2L_d}{4r_1^2G_m}\\&\cdot[4r_2^4\ln(r_2/r_1)+4r_1^2r_2^2-r_1^4-3r_2^4],\end{aligned}\tag{26}$$

$$\begin{aligned}U_{ed}=&\int_{L_d}^{L}\int_0^{r_1}\left[\frac{(\sigma_f^z(z))^2}{2E_f}+\frac{(\tau_f^{rz}(r,z))^2}{2G_f}\right]2\pi r\mathrm{d}r\mathrm{d}z\\&+\int_{L_d}^{L}\int_{r_1}^{r_2}\left[\frac{(\sigma_m^z(r,z))^2}{2E_m}+\frac{(\tau_m^{rz}(r,z))^2}{2G_m}\right]2\pi r\mathrm{d}r\mathrm{d}z\\=&\frac{\pi r_1^2}{2E_f}[C^2/(2\beta)+(\sigma_f^\infty)^2(L-L_d)+2C\sigma_f^\infty/\beta]\\&+\frac{\pi C^2\beta r_1^4}{32G_f}+\frac{\pi(r_2^2-r_1^2)}{2E_m}[\lambda^2C^2/(2\beta)\\&+(\sigma_m^\infty)^2(L-L_d)-2\lambda C\sigma_m^\infty/\beta]\\&+\frac{\pi\lambda^2C^2\beta[4r_2^4\ln(r_2/r_1)+4r_1^2r_2^2-r_1^4-3r_2^4]}{32G_m},\end{aligned}\tag{27}$$

where $G_i(i=f,m)$ are the shear moduli of fiber and matrix and $G_i=E_i/[2(1+\nu_i)]$.

The axial displacements in the fiber and matrix are calculated respectively by

$$\begin{aligned}w_f(z)=&\int_z^{L_d}\frac{\sigma_b-2\tau_sz/r_1}{E_f}\mathrm{d}z+\int_{L_d}^{L}\frac{\sigma_f^z(z)}{E_f}\mathrm{d}z\\=&\frac{\sigma_b}{E_f}(L_d-z)-\frac{\tau_s(L_d^2-z^2)}{r_1E_f}\\&+\frac{C}{E_f\beta}+\frac{\sigma_f^\infty}{E_f}(L-L_d),\end{aligned}\tag{28}$$

$$\begin{aligned}w_m(z)=&\int_z^{L_d}\frac{2\lambda\tau_sz/r_1}{E_m}\mathrm{d}z+\int_{L_d}^{L}\frac{\sigma_m^z(r,z)}{E_m}\mathrm{d}z\\=&\frac{\lambda\tau_s(L_d^2-z^2)}{r_1E_m}-\frac{\lambda C}{E_m\beta}\\&+\frac{\sigma_m^\infty}{E_m}(L-L_d),\end{aligned}\tag{29}$$

where the effects of exponential terms at $L\to\infty$ are neglected. The directions of $w_f(z)$ and $w_m(z)$ are contrary to the z axis.

The relative axial displacement $v(z)$ between the fiber and the matrix is calculated by

$$\begin{aligned}v(z)=&|w_f(z)-w_m(z)|\\=&-\frac{E_c\tau_s}{r_1E_fE_mV_m}(L_d^2-z^2)+\frac{\sigma_b}{E_f}(L_d-z)\\&+\frac{CE_c}{E_fE_mV_m\beta},\end{aligned}\tag{30}$$

where the far-field axial strain in the fiber is equal to that in the matrix, and the expression $\sigma_f^\infty/E_f=\sigma_m^\infty/E_m$ approximatedly holds.

The work U_f done by the friction stress τ_s at the debonded interface is calculated by

$$\begin{aligned}U_f=&2\pi r_1\int_0^{L_d}\tau_s[v(z)-u_{shear}]\mathrm{d}z\\=&2\pi r_1\left[-\frac{2E_c\tau_s^2L_d^3}{3r_1E_fE_mV_m}+\frac{\sigma_b\tau_sL_d^2}{2E_f}\right.\\&\left.+\frac{CE_c\tau_sL_d}{E_fE_mV_m\beta}-\frac{r_1\tau_s^2\phi L_d}{2G_m}\right],\end{aligned}\tag{31}$$

where $u_{shear}=\tau_sr_1\phi/(2G_m)$ is the contribution of the matrix shear deformation to the crack opening displacement. ϕ is a nondimensional parameter and expressed as[15]

$$\phi=-[2\ln V_f+V_m(3-V_f)]/(2V_m^2).\tag{32}$$

The work U_w done by the pull-out stress σ_b is expressed as

$$U_w=\pi r_1^2\sigma_bU_{debond}.\tag{33}$$

Here, U_{debond} is the additional displacement of composite due to interfacial debonding and defined as the difference between the fiber displacement $w_f(z)$ at the fiber loaded end $z=0$ and the composite displacement w_c in the absence of interfacial debonding

$$\begin{aligned}U_{debond}=&w_f(0)-w_c=w_f(0)-\sigma_f^\infty L/E_f\\=&\frac{\sigma_bL_d}{E_f}-\frac{\tau_sL_d^2}{r_1E_f}+\frac{C}{E_f\beta}-\frac{\sigma_f^\infty L_d}{E_f},\end{aligned}\tag{34}$$

where the far-field axial strain in the fiber is equal to that in the composite at $L\to\infty$.

According to the fracture mechanics, interfacial debonding can be considered as II-type crack growth. The interfacial debonding energy U_s changes by a factor $2\pi r_1\cdot\mathrm{d}L_d$ as the interface crack with the length of L_d advances a length $\mathrm{d}L_d$.

Combination of Eqs. (25)—(27), (31) and (33) leads to the solution of the energy release rate G

$$G = \frac{1}{2\pi r_1}\frac{\partial U_s}{\partial L_d} = \lambda_1 L_d^2 + \lambda_2 L_d + \lambda_3,$$

$$\lambda_1 = \frac{E_c\tau_s^2}{r_1 E_f V_m E_m},$$

$$\lambda_2 = \frac{3E_c\tau_s^2}{r_1\beta E_f E_m V_m} - \frac{r_1\beta\tau_s^2}{8G_f} - \frac{\lambda_4\lambda^2\beta\tau_s^2}{8r_1^3 G_m} - \frac{\sigma_b\tau_s}{E_f},$$

$$\lambda_3 = \frac{r_1\sigma_b^2}{4E_f} + \frac{r_1(\sigma_f^\infty)^2}{4E_f} - \frac{r_1\sigma_b\sigma_f^\infty}{2E_f} - \frac{\tau_s(\sigma_b - \sigma_f^\infty)}{E_f\beta} - \frac{E_c\tau_s(\sigma_b - \sigma_f^\infty)}{2E_f E_m V_m\beta} + \frac{\tau_s\sigma_m^\infty}{E_m\beta} + \frac{r_1(\sigma_m^\infty)^2}{4\lambda E_m} + \frac{\beta r_1^2\tau_s(\sigma_b - \sigma_f^\infty)}{16G_f} - \frac{r_1\tau_s^2}{8G_f} + \frac{r_1\phi\tau_s^2}{2G_m} + \frac{\lambda_4\lambda^2\beta\tau_s(\sigma_b - \sigma_f^\infty)}{16r_1^2 G_m} - \frac{\lambda_4\lambda^2\tau_s^2}{8r_1^3 G_m},$$

$$\lambda_4 = 4r_2^4\ln(r_2/r_1) + 4r_1^2r_2^2 - r_1^4 - 3r_2^4. \quad (35)$$

Eq. (35) shows that the energy release rate G is a second-order function of the debond length L_d when the material- and geometry- parameters are given. By introducing an interfacial debonding criterion $G \geqslant \Gamma_i$, the critical debond length can be determined by solving Eq. (35):

$$L_{d1,2} = \frac{-\lambda_2 \pm \sqrt{\lambda_2^2 - 4\lambda_1(\lambda_3 - \Gamma_i)}}{2\lambda_1}. \quad (36)$$

For the two roots above, only the smaller one L_{d1} is physically meaningful and we will discuss it below.

Compared with Eq. (35), if the thermal effect is neglected, the results obtained by Hsueh[8] and Chiang[14] are respectively

$$G = \frac{r_1 V_m E_m}{4E_f E_c}\left(\sigma_b - \frac{2\tau_s E_c L_d}{r_1 V_m E_m}\right)^2 = \frac{E_c\tau_s^2}{r_1 E_f V_m E_m}L_d^2 - \frac{\sigma_b\tau_s}{E_f}L_d + \frac{r_1 E_m V_m\sigma_b^2}{4E_c E_f}, \quad (37)$$

$$G = \frac{E_c\tau_s^2}{r_1 E_f V_m E_m}L_d^2 + \left(\frac{E_c\tau_s^2}{\eta E_f V_m E_m} - \frac{\sigma_b\tau_s}{E_f}\right)L_d + \frac{r_1 E_m V_m\sigma_b^2}{4E_c E_f} - \frac{r_1\sigma_b\tau_s}{2\eta E_f}, \quad (38)$$

$$\eta^2 = \frac{4E_c G_m}{V_m E_m E_f\phi}. \quad (39)$$

According to Marshall[16], for parallel bridging fibers in matrix crack growth, the bridging constitutive relationship is described as the relationship between the bridging traction $T(x)$ and the half COD profile $u(x)$. From Eqs. (30) and (36), we obtain

$$v(0) = -\frac{E_c\tau_s}{r_1 E_f E_m V_m}L_{d1}^2 + \left(\frac{\sigma_b}{E_f} - \frac{2\tau_s E_c}{r_1\beta E_f E_m V_m}\right)L_{d1} + \frac{(\sigma_b - \sigma_f^\infty)E_c}{E_f E_m V_m\beta}, \quad (40)$$

$$u = \frac{E_m V_m}{E_c}v(0), \quad T(x) = \sigma_b(x)V_f. \quad (41)$$

Compared with Eq. (40), if the thermal effect is neglected, the result obtained by Hsueh[8] is

$$v(0) = \frac{r_1 V_m E_m\sigma_b^2}{4E_f E_c\tau_s} - \frac{\Gamma_i}{\tau_s}. \quad (42)$$

5 Results and discussion

The fiber-reinforced composite SiC/Ti-6Al-4V and software Maple9 were adopted in numerical calculations. The parameters used in the calculations are: $E_f = 400$ GPa, $E_m = 115$ GPa, $\nu_f = 0.17$, $\nu_m = 0.3$[17], $\alpha_f^T = 2.63 \times 10^{-6}$ ℃, $\alpha_f^L = 5 \times 10^{-6}$ ℃, and $\alpha_m^T = \alpha_m^L = 10 \times 10^{-6}$ ℃[18]. The fiber tensile strength $\sigma_s = 4.19$ GPa, the interfacial shear strength $\tau_u = 120$ MPa[19]. The fiber radius $r_1 = 10\ \mu$m, the matrix radius $r_1 = 100\ \mu$m, and the fiber volume fraction $V_f = 1\%$.

Fig. 3 shows distributions of the energy release rate G versus the normalized debond length L_d/r_1 without the thermal effect. Theoretically, it should be pointed out that the friction stress τ_s affects G in the form of $E_c\tau_s^2/(r_1 E_f V_m E_m)$ in Eqs. (35), (37) and (38), and the energy release rate decreases and then re-increases with the increase of L_d/r_1. However, the re-increasing part is physically meaningless because interfacial debonding appears only at $G > \Gamma_i$ (here, the interfacial debonding toughness is assumed as $\Gamma_i = 1$ J/m^2) and stops when the condition $G = \Gamma_i$ is satisfied at some applied pull-out stress σ_b. Therefore, the critical debond length is taken as the smaller one L_{d1} in Eq. (36). The conclusion was also verified by Liu[9]. However, Liu's conclusion was based on the Lamé method, suffering from similar setbacks to that in the shear-lag models. The G values obtained by us are smaller than those obtained by Hsueh and Chiang at the same L_d/r_1, because Hsueh neglected the shear and radial stresses, the shear strain energy in the fiber and matrix, the variation of axial stress in

the matrix with radial positions, and the Poisson's effect, and Chiang only further considered the shear strain energy in the matrix.

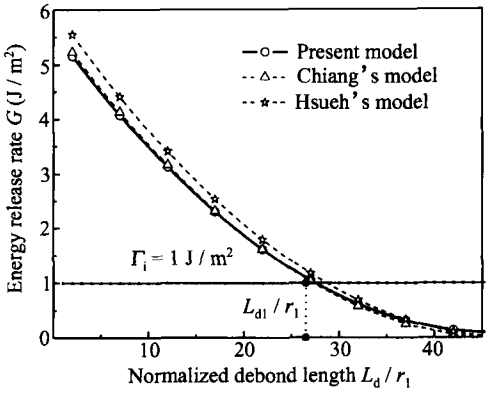

Fig. 3. Distributions of the energy release rate G versus the normalized debond length L_d/r_1 at the pull-out stress $\sigma_b = 1$ GPa, the temperature change $\Delta T_p = 0$ and the friction stress $\tau_s = 10$ MPa.

Fig. 4 illustrates the effect of friction stress τ_s on the energy release rate G without the thermal effect. In terms of different friction stress τ_s, the differences between the G values are relatively small when L_d/r_1 is small, and become large at larger L_d/r_1. At the same L_d/r_1, increasing friction stress τ_s results in smaller G, and longer debond length before interface failure. The $G \sim L_d/r_1$ curve tends to be a horizontal line when the friction stress τ_s decreases and approaches the minimum value $\tau_s = 0$. The energy release rate reaches the maximum value $G = 6.02$ J/m^2 at $\tau_s = 0$, showing the weakest ability for the interface to resist failure.

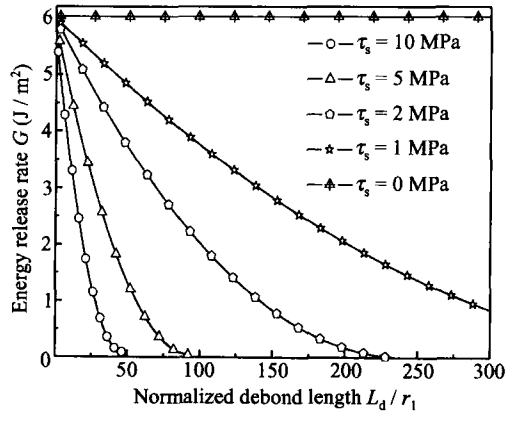

Fig. 4. Distributions of the energy release rate G versus the normalized debond length L_d/r_1 at the pull-out stress $\sigma_b = 1$ GPa, the temperature change $\Delta T_p = 0$, and the friction stress $\tau_s = 0$ MPa, 1 MPa, 2 MPa, 5 MPa, and 10 MPa, respectively.

Fig. 5 illustrates the effect of pull-out stress σ_b on the energy release rate G without the thermal effect. The $G \sim L_d/r_1$ curve tends to be a horizontal line at low σ_b. At the same L_d/r_1, G is larger for higher σ_b, which was also obtained by Wu[20] by applying the principle of minimum potential energy at low strain levels. The difference lies in that theoretically no re-increasing tendency appears in the $G \sim L_d/r_1$ curves obtained by Wu.

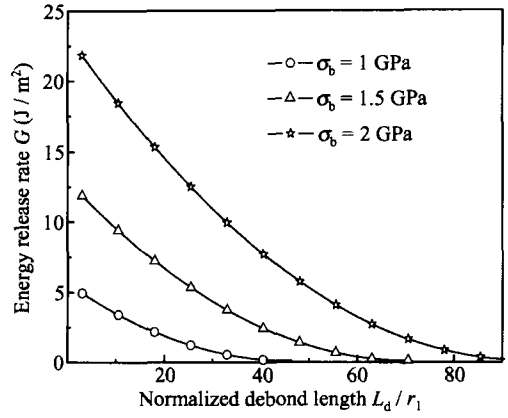

Fig. 5. Distributions of the energy release rate G versus the normalized debond length L_d/r_1 at the friction stress $\tau_s = 10$ MPa, the temperature change $\Delta T_p = 0$, and the pull-out stress $\sigma_b = 1$ GPa, 1.5 GPa, and 2 GPa, respectively.

Fig. 6 illustrates the effect of temperature change ΔT_p on the energy release rate G. It can be seen that larger ΔT_p can result in smaller G and can slow down the interface failure. By applying the shear-strength-based criterion, Quek[13] obtained the same conclusion. In Eq. (35), the thermal effect is represented by the far-field fiber axial stress σ_f^∞. Then, in Eqs. (18), (19) and (21), σ_f^∞ increases and then the shear stress $\tau_i(z)$ at the bonded interface decreases with the increasing $|\Delta T_p|$.

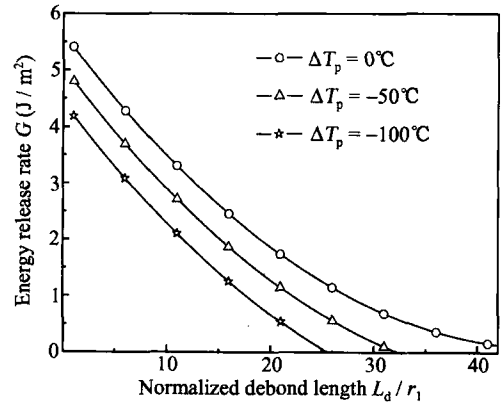

Fig. 6. Distributions of the energy release rate G versus the normalized debond length L_d/r_1 at the friction stress $\tau_s = 10$ MPa, the pull-out stress $\sigma_b = 1$ GPa, and the temperature change $\Delta T_p = 0$ ℃, -50 ℃, and -100 ℃, respectively.

Fig. 7 shows the bridging constitutive relationship between the bridging traction $T(x)$ and the half COD profile $u(x)$ without the thermal effect. The appearance of positive $u(x)$ requires the increase of bridging traction $T(x)$ to a critical value to overcome the friction stress τ_s. The $T(x)$ values are slightly smaller than that obtained by Hsueh at the same $u(x)$ value, showing a stronger ability to resist the interface failure with the increase of τ_s. The conclusion can also be directly deduced from Eq. (35): the shear effects in the fiber and matrix and the Poisson's effect, neglected by the shear-lag models, become more remarkable with the increase of τ_s.

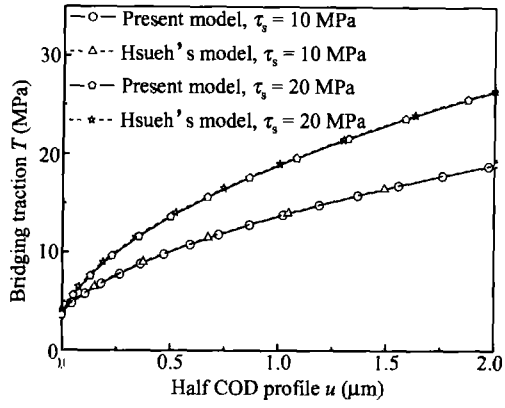

Fig. 7. Bridging constitutive relationships at the temperature change $\Delta T_p = 0$, the interfacial debonding toughness $\Gamma_i = 1$ J/m^2, and the friction stress τ_s = 10 MPa and 20 MPa, respectively.

Fig. 8 illustrates the effect of friction stress τ_s on the bridging constitutive relationship without the thermal effect. $T(x)$ increases with the increasing friction stress τ_s at $u > 0$. Because the fiber tensile strength $\sigma_s = 4.19$ GPa, from Eq. (41), the maximum bridging traction $T = 40.19$ MPa. Before the friction stress τ_s reaches the interfacial shear strength τ_u, the fiber axial stress may exceed the fiber tensile strength and fibers will break. Therefore, an optimum interface exists for obtaining a maximum interfacial debonding toughness Γ_i.

Fig. 9 illustrates the effect of interfacial debonding toughness Γ_i on the bridging constitutive relationship without the thermal effect. The curves $T(x) \sim u(x)$ start at the origin at $\Gamma_i = 0$ J/m^2, which is also directly obtained from Eq. (36). $T(x)$ increases with the increasing Γ_i at the same $u(x)$. The $T(x) \sim u(x)$ curve tends to be a horizontal line with the increase of Γ_i, showing a stronger ability to resist the interface failure.

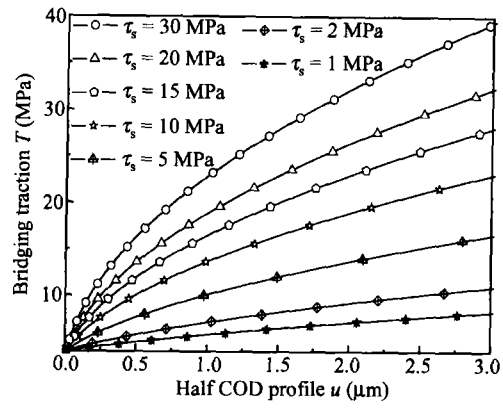

Fig. 8. Bridging constitutive relationships at the temperature change $\Delta T_p = 0$, the interfacial debonding toughness $\Gamma_i = 1$ J/m^2, and the friction stress τ_s = 1 MPa, 2 MPa, 5 MPa, 10 MPa, 15 MPa, 20 MPa, and 30 MPa, respectively.

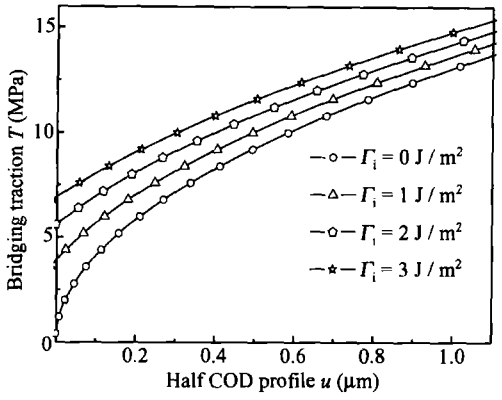

Fig. 9. Bridging constitutive relationships at the temperature change $\Delta T_p = 0$, the friction stress $\tau_s = 10$ MPa, and the interfacial debonding toughness $\Gamma_i = 0$ J/m^2, 1 J/m^2, 2 J/m^2, and 3 J/m^2, respectively.

Fig. 10 illustrates the effect of temperature change ΔT_p on the bridging constitutive relationship. The bridging traction $T(x)$ increases at large $|\Delta T_p|$, showing that the thermal residual stresses resulting from temperature drop can help to slow down the interface failure.

Generally, fiber bridging can be divided into three distinctive microscopic processes: (a) fiber bridging without frictional sliding at the debonded interface, (b) frictional bridging associated with interfacial debonding and frictional sliding at the interface, and (c) pull-out bridging accompanied by fibers failure. The above three continuous processes are consistent with the transformation process from fiber bridging, fiber failure to fiber pullout, indicating an appropriate strain hardening followed by a strain softening. However, the third process on pull-out bridging is not

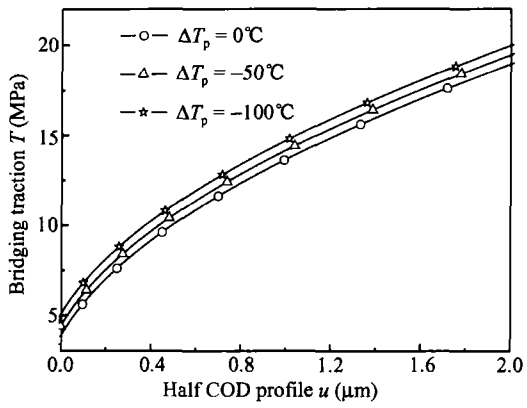

Fig. 10. Bridging constitutive relationships at the friction stress $\tau_s = 10$ MPa, the interfacial debonding toughness $\Gamma_i = 1$ J/m^2, and the temperature change $\Delta T_p = 0$ ℃, -50 ℃, and -100 ℃, respectively.

included in Figs. 7—10 and interface failure is not considered.

As to the frictional bridging, the bridging constitutive relationship for determining the bridging traction $T(x)$ obtained from the half COD profile $u(x)$ was expressed as[15,16]

$$T(x) = a + bu(x)^n, \qquad (43)$$

where the coefficients a, b, n are constants correlated to the material- and geometry- parameters, and the interfacial properties, etc.

By applying a mechanical balance between the external tensile stress and the internal bridging stress, Marshall[16] found the power exponent $n = 0.5$, which shows that $T(x)$ increases with the square root increase of $u(x)$.

By fitting a series of discrete data, in Fig. 8, the power exponents are calculated as $n = 0.50048$, 0.50056, 0.50083, 0.50135, 0.50193, 0.50260, and 0.50414 at the friction stress $\tau_s = 1$ MPa, 2 MPa, 5 MPa, 10 MPa, 15 MPa, 20 MPa, and 30 MPa, respectively; in Fig. 9, $n = 0.50865$, 0.50135, 0.49352, and 0.48565 at the interfacial debonding toughness $\Gamma_i = 0$ J/m^2, 1 J/m^2, 2 J/m^2, and 3 J/m^2, respectively. The friction stress τ_s has less remarkable effect on the power exponent n than the interfacial debonding toughness Γ_i. On the one hand, from Eqs. (35), (36), (40) and (41), the interrelationship between the bridging traction $T(x)$ and the half COD profile $u(x)$ becomes lower at $\tau_s \to 0$ and is equal to zero at $\tau_s = 0$, corresponding to the case of no fiber bridging. On the other hand, for a strong interface with high friction stress τ_s, more axial and shear deformations in the fiber and matrix occur and more fibers fail, deviating the power exponent from the value $n = 0.5$. Therefore, the power law relationship $n = 0.5$ is more acceptable in the case of a weak interface with relatively low friction stress τ_s and interfacial debonding toughness Γ_i than in a strong interface case.

6 Conclusions

In this paper, an improved theoretical model simulating the properties of frictional bridging is presented by using stress equilibrium equations, including the friction at the debonded interface and the thermal effect, and relatively perfect stress solutions in the fiber and matrix are obtained. Based on the energy equilibrium, an expression for the energy release rate G is derived. By introducing an interfacial debonding criterion $G \geqslant \Gamma_i$, the bridging constitutive relationship is obtained. Numerical calculations are carried out for the fiber-reinforced composite SiC/Ti-6Al-4V to explore the effects of related parameters and the results are also compared with those obtained by using other existing models. In summary,

1) A method for determining the critical debond length is obtained based on the interfacial debonding criterion $G \geqslant \Gamma_i$.

2) The $G \sim L_d$ curve tends to be a horizontal line when the friction stress τ_s decreases and approaches zero, where the energy release rate G becomes a constant independent of the debond length L_d.

3) Theoretically, the curves $G \sim L_d$ display the first decreasing and then re-increasing tendency. However, the re-increasing part is physically meaningless because interfacial debonding appears only at $G > \Gamma_i$, and stops when the condition $G = \Gamma_i$ is satisfied.

4) With the increase of friction stress τ_s, the shear effects in the fiber and matrix and Poisson's effect, neglected by the shear-lag models, become more remarkable for suppressing the interface failure.

5) The thermal residual stresses due to the fiber/matrix thermal mismatch can slow down the interface failure.

6) The power exponent $n = 0.5$ is more acceptable in the case of a weak interface with relatively low

friction stress τ_s and interfacial debonding toughness Γ_i than in a strong interface case.

References

1 Begley M.R. and McMeeking R.M. Fatigue crack growth with fiber failure in metal-matrix composites. Comp. Sci. Technol., 1995, 53(4): 365—382.

2 Begley M.R. and McMeeking R.M. Numerical analysis of fibre bridging and fatigue crack growth in metal matrix composite materials. Materials Science and Engineering: A, 1995, 200(1—2): 12—20.

3 Hampe A., Kalinka G., Meretz S. et al. An advanced equipment for single-fibre pull-out test designed to monitor the fracture process. Composites, 1995, 26(1): 40—46.

4 Piggott M.R. A new model for interface failure in fibre-reinforced polymers. Comp. Sci. Technol., 1995, 55(3): 269—276.

5 Honda K. and Kagawa Y. Debonding criterion in the pushout process of fiber-reinforced ceramics. Acta Materialia, 1996, 44(8): 3267—3277.

6 Honda K. and Kagawa Y. Analysis of shear stress distribution in pushout process of fiber-reinforced ceramics. Acta Metallurgica Materialia, 1995, 43(4): 1477—1487.

7 Jiang X.Y. and Gao Q. Stress-transfer analysis for fibre/matrix interfaces in short-fibre-reinforced composites. Comp. Sci. Technol., 2001, 61(10): 1359—1366.

8 Hsueh C.H. Crack-wake interfacial debonding criteria for fiber-reinforced ceramic composites. Acta Materialia, 1996, 44(6): 2211—2216.

9 Liu Y.F. and Kagawa Y. The energy release rate for an interfacial debond crack in a fiber pull-out model. Comp. Sci. Technol., 2000, 60(2): 167—171.

10 Chiang Y.C. On crack-wake debonding in fiber reinforced ceramics. Engineering Fracture Mechanics, 2000, 65(1): 15—28.

11 Rauchs G. and Withers P.J. Computational assessment of the influence of load ratio on fatigue crack growth in fibre-reinforced metal matrix composites. International Journal of Fatigue, 2002, 24(12): 1205—1211.

12 Rauchs G., Thomason P.F. and Withers P.J. Finite element modelling of frictional bridging during fatigue crack growth in fibre-reinforced metal matrix composites. Computational Materials Science, 2002, 25(1—2): 166—173.

13 Quek M.Y. Stress transfer at a partially bonded fibre/matrix interface. International Journal of Adhesion and Adhesives, 2002, 22(4): 303—310.

14 Chiang Y.C. On fiber debonding and matrix cracking in fiber-reinforced ceramics. Comp. Sci. Technol., 2001, 61(12): 1743—1756.

15 Budiansky B., Evans A.G. and Hutchinson J.W. Fiber-matrix debonding effects on cracking in aligned fiber ceramic composites. International Journal of Solids and Structures, 1995, 32(3—4): 315—328.

16 Marshall M.B. A J-integral method for calculating steady-state matrix cracking stresses in composites. Mechanics of Materials, 1988, 7(1): 127—136.

17 Preuss M., Rauchs G., Doel T.J.A. et al. Measurements of fibre bridging during fatigue crack growth in Ti/SiC fibre metal matrix composites. Acta Materialia, 2003, 51(4): 1045—1057.

18 Honda K., Kagawa Y. and Mai Y.W. Effects of relative sliding distance on the frictional stress transfer in fiber-reinforced ceramics. Materials Science and Engineering: A, 1998, 252(1): 53—63.

19 Warrier S.G., Maruyama B., Majumdar B.S. et al. Behavior of several interfaces during fatigue crack growth in SiC/Ti-6Al-4V composites. Materials Science and Engineering: A, 1999, 259(2): 189—200.

20 Wu W., Verpoest I. and Varna J. Prediction of energy release rate due to the growth of an interface crack by variational analysis. Comp. Sci. Technol., 2000, 60(3): 351—360.